# Multifunctional Nanofibrous Scaffolds Capable of Localized Delivery of Theranostic Nanoparticles for Postoperative Cancer Management

*Lin Guo[1,†], Qilong Zhao[1,2,†], Li-wu Zheng[3], Min Wang[1,*]*

[1] Department of Mechanical Engineering, The University of Hong Kong, Pokfulam Road, Hong Kong
[1,2] Institute of Biomedical & Health Engineering, Shenzhen Institute of Advanced Technology (SIAT), Chinese Academy of Sciences (CAS), Shenzhen 518055, China
[3] Faculty of Dentistry, The University of Hong Kong 34 Hospital Road, Sai Ying Pun, Hong Kong

†These authors contributed equally to this work.
*Corresponding authors. E-mail: memwang@hku.hk

## Abstract

Postoperative recovery of cancer patients can be affected by complications such as tissue dysfunction or disability caused by tissue resection and also cancer recurrence resulting from residual cancer cells. Despite impressive progresses made for tissue engineering scaffolds that assist tissue regeneration for postoperative cancer patients, the majority of existing tissue engineering scaffolds still lacks functions for monitoring and killing residual cancer cells, if there are any, upon their detection. In this study, we have developed multifunctional scaffolds that comprise biodegradable nanofibers and core-shell structured microspheres encapsulated with theranostic nanoparticles (NPs). The multifunctional scaffolds possess an extracellular matrix (ECM)-like nanofibrous architecture and soft tissue-like mechanical properties, making them excellent tissue engineering patch candidates for assisting the repair and regeneration of tissues at the cancerous sites after surgery. Furthermore, they are capable of localized delivery of theranostic NPs upon quick degradation of core-shell structured microspheres that contain the theranostic NPs. Leveraging on folic acid (FA)-mediated ligand-receptor binding, surface

enhanced Raman scattering (SERS) activity and near infrared (NIR)-responsive photothermal effect of the theranostic gold NPs (AuNPs) delivered locally, the multifunctional scaffolds display excellent active targeting, diagnosis, and photothermal therapy functions for cancer cells, showing great promise for adaptive postoperative cancer management.

**Keywords:** Multifunctional scaffold; tissue engineering; theranostic; electrospinning; postoperative cancer management

## 1. Introduction

Cancer has become a major threat to human lives. It has been estimated that worldwide there are approximately 14.1 million new cases of cancer and that nearly 8.2 million people die from cancer each year[1]. In hospitals, surgical removal of tumors is one of the most frequently used and also highly effective methods for treating cancers, particularly solid tumors[2]. However, the postoperative recovery is still far from satisfactory for many cancer patients[3], which is very often accompanied by a much lowered quality of life caused by tissue dysfunction or disability after the removal of tumor together with surrounding healthy tissue and/or high risk of cancer recurrence due to incomplete elimination of cancer cells[4, 5]. Conventionally, postoperative radiotherapy and/or chemotherapy are provided to patients for reducing the risk of cancer recurrence[6, 7], while their inevitable side effects can impair wound healing and the repair/regeneration of tissue at the resection site[8]. For achieving much improved and desired postoperative cancer management, it is necessary to develop adaptive strategies that can simultaneously promote tissue repair/regeneration, detect residual cancer cells/cancer recurrence and kill the cancer cells on demand when they are detected[9].

Electrospun scaffolds, which provide nanofibrous architectures that resemble nanofibrous structures of extracellular matrix (ECM) of human body tissues and can therefore act as desirable artificial microenvironments for cell attachment and cell growth[10-12], have shown their high attractiveness in assisting the repair/regeneration of tissues at original tumor site after surgery[13, 14]. Moreover, functional agents such as small-molecule drugs and therapeutic nano-systems can be incorporated relatively easily in electrospun scaffolds through chosen electrospinning techniques, thereby imparting the scaffolds with additional functions for preventing cancer recurrence[15]. For example, nanofibrous scaffolds incorporated with anti-cancer drugs (e.g., doxorubicin) and/or therapeutic nano-agents (e.g., black phosphorus or MXene nanosheets) have been made and studied[16-19], and these scaffolds showed the potential for synergistic postoperative cancer management by promoting tissue repair/regeneration and providing concurrent chemo-photothermal therapy. However, there is still the lack of an integrated diagnosis-to-therapy capability with the scaffolds, and hence such nanofibrous scaffolds may cause similar side effects like the conventional postoperative radiotherapy and/or chemotherapy.

In recent decades, a variety of nanoparticles (NPs) with unique structural and physical characteristics, such as silica NPs[20], magnetic NPs[21] and noble metallic NPs[22], have been made, and they have attracted increasing attention in the biomedical field owing to their great promise as cancer theranostics which can provide both diagnostic and therapeutic functions for cancers. Among them, gold NPs (AuNPs) are particularly attractive due to their little or no long-term cytotoxicity[23]. Additionally, by tailoring their shapes and/or through surface functionalization, AuNPs can be equipped with multiple enhanced functions, including selectively binding to

cancer cells based on both passive targeting through trans-endothelial pathways[24] and active targeting through interactions between the surface functionalized ligands on AuNPs and receptors on cancer cell surfaces[25], sensitive sensing and imaging of cancer cells via amplified Raman signals based on the surface enhanced Raman scattering (SERS) effect for the embedded Raman reporter molecules[26, 27], and effective ablation of cancer cells through photothermal effect resulting from surface plasmon resonance (SPR) absorption of AuNP in the near infrared (NIR) region[28-30]. Our group has developed a targeting-sensing-photothermal therapy (PTT) three-in-one cancer theranostic based on AuNP[31], which contains a highly branched AuNP core and a conjugated folic acid (FA)-chitosan (CS) polymeric shell that is embedded with SERS reporter molecules. The conjugated FA in the polymeric shell empowers this nanotheranostic for active targeting for cancer cells over-expressing folate receptors[32], subsequently selectively sensing and then killing the cancer cells through, respectively, SERS detection and NIR-mediated PTT. In spite of achieving this integrated diagnosis-to-therapy capability, challenges, such as short circulation time *in vivo*[33], remain for using such theranostic NPs in postoperative cancer managements. Combining tissue engineering scaffolds with theranostic NPs can be a viable strategy for addressing respective shortcomings of current tissue engineering scaffolds that do not have the diagnosis-and-therapy capability and theranostic NPs that are rapidly cleared out from the body. However, it is a highly demanding task to achieve high-efficiency encapsulation and then localized delivery of nano-sized theranostics with well-preserved structures and functions for multifunctional tissue engineering scaffolds[34].

Recently, our group showed that biodegradable core-shell structured microspheres could be made via coaxial electrospraying[35]. Such core-shell structured microspheres could provide desirable reservoirs for the controlled delivery of a variety of cargos of different scales, ranging from macromolecular growth factors to mammalian cells[35, 36], where the bioactivity of growth factors and viability of cells could be well preserved. Notably, coaxial electrospraying is easily integrated with electrospinning[36], thus offering a possible route for forming multifunctional nanofibrous scaffolds capable of delivering nano-sized cargos such as theranostic NPs. In the current study, rhodamine 6G (R6G)-embedded and CS-FA-capped highly branched AuNPs as theranostic NPs (Fig. 1a) were firstly synthesized according to our previous work[31], which were then encapsulated in biodegradable core-shell structured microspheres and integrated with electrospun nanofibers to form multifunctional scaffolds through concurrent coaxial electrospraying and electrospinning (Fig. 1b). Poly(lactic-*co*-glycolic acid) polymers with an LA-to-GA molar ratio of 75:25 (PLGA75/25) and 50:50 (PLGA50/50), which are U.S. Food and Drug Administration (FDA)-approved biodegradable polymers, were employed for making electrospun nanofibers and coaxial electrosprayed microspheres, respectively. Owing to relatively rapid degradation of PLGA50/50 polymer in the body, the encapsulated theranostic NPs would be gradually released from biodegraded microspheres while the PLGA75/25 polymer scaffolds could maintain their nanofibrous architectures and also mechanical stability. Through the controlled local delivery of theranostic AuNPs which provides an equivalent of a prolonged circulation time of at least 21 days, the new nanofibrous scaffolds exhibited multiple functions, including active targeting of the targeted cancer cells, SERS-assisted cancer detection, and NIR-mediated PTT for cancer (Fig. 1c), along with their

major function of tissue regeneration. Such multifunctional nanofibrous scaffolds should satisfy the comprehensive requirements of promoting tissue regeneration and providing cancer detection and cancer therapy, when needed, thereby offering the desirable adaptive postoperative cancer management.

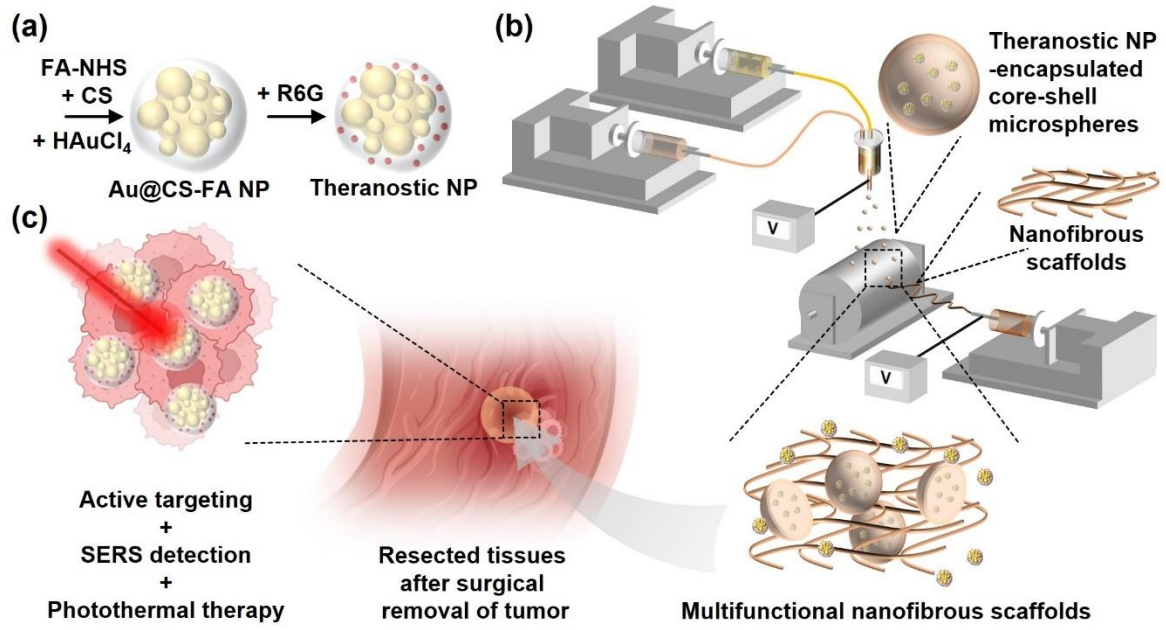


**Figure 1 Schematic illustrations for the design and fabrication of multifunctional nanofibrous scaffolds, enabling localized delivery of theranostic NPs for postoperative cancer managements.** (a) Synthesis of theranostic AuNP. The theranostic AuNP contains a highly branched AuNP core, a CS-FA-conjugated polymeric shell, and embedded R6G reporter molecules. (b) Fabrication of multifunctional nanofibrous scaffolds through concurrent electrospinning and coaxial electrospraying. (c) Postoperative cancer management by using the multifunctional nanofibrous scaffolds. The multifunctional nanofibrous scaffolds are used as a tissue engineering patch at the resection site after surgical removal of

the tumor. The local delivery of theranostic NPs from multifunctional scaffolds upon breakup of core-shell structured microspheres will realize active targeting, SERS-based detection and PTT for possible residual cancer cells, thus preventing cancer recurrence.

## 2. Results and Discussion

### 2.1 Formation, characteristics, and microencapsulation of theranostic NPs

The multiple functions (active targeting, cancer detection, and photothermal cancer therapy) to be achieved for the multifunctional scaffolds in this study depended on the realization of multiple functions of theranostic AuNPs to be delivered via coaxial electrosprayed microspheres that had been incorporated in the nanofibrous matrix of these scaffolds. Given that the unique characteristics (e.g., structure, SERS activity, and SPR adsorption) of the theranostic AuNPs were the prerequisites for their diagnostic and therapeutic functions, the synthesized theranostic AuNPs were firstly characterized from different aspects. The theranostic NPs used in the current investigation were R6G-embedded and CS-FA-capped AuNPs, which were made according to our previous work owing to their high promises for cancer detection and therapy[31, 37]. With TEM examination and size distribution analysis, it was observed that as-synthesized AuNPs had good monodispersity and uniform structures, with a narrow size distribution mainly from 60 to 110 nm (Fig. S1). The existence of an AuNP core and successful embedding of R6G (with strong inherent red fluorescence) in the CS-FA shell in the theranostic AuNPs were revealed by the dark-field microscopy (Fig. S2a) and fluorescence microscopy (Fig. S2b), respectively. The TEM images showed the core-shell

structure of these theranostic AuNPs, which contained a highly branched AuNP core with many irregular tips (Fig. 2a) and a thin layer of polymeric shell (Fig. 2b). The highly branched AuNP core was needed for generating strong SERS effects (Fig. 2c), because the SERS substrate of nanoscale surface roughness of Au (herein the AuNP core) would enhance its coupling with the Raman reporter molecules (herein the R6G) and consequently result in the desired high SERS signals [38] that the theranostic AuNPs must produce. Furthermore, the highly branched structure of the AuNP cores had also contributed to the broad region of the wavelength of these theranostic NPs, ranging from 500 to 900 nm (Fig. S3) due to their high aspect ratios[31], for their strong SPR absorption. Since this region of the wavelength is inside the biological transparency NIR-infrared light window that permits deep penetration of light across biological tissues[39], the AuNPs that had been fabricated and would be used in multifunctional scaffolds would be an excellent therapeutic agent to provide NIR-mediated photothermal cancer therapy.

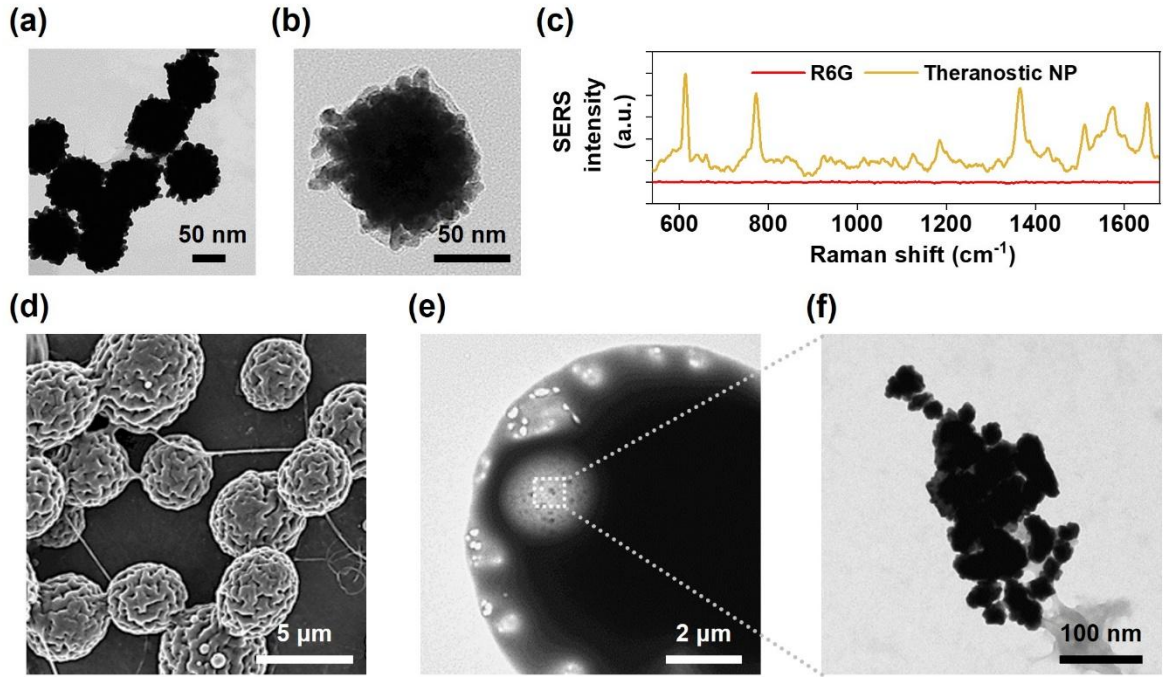

**Figure 2 Formation, characteristics, and microencapsulation of theranostic AuNPs.** (a) A representative TEM image (low magnification) of theranostic AuNPs showing the highly branched structure of the AuNP core. (b) A representative TEM image (high magnification) of theranostic AuNPs showing a thin layer of polymeric shell. (c) SERS spectra of the neat R6G molecules and R6G-containing theranostic AuNPs. (d) Morphology and spherical structure of theranostic AuNP-encapsulated PLGA50/50 microspheres formed by coaxial electrospraying. (e) A representative TEM image (low magnification) showing the core-shell structure of theranostic AuNP-encapsulated PLGA50/50 microspheres. (f) A representative TEM image (high magnification) confirming the existence of theranostic AuNPs encapsulated in coaxial electrosprayed PLGA50/50 microspheres.

Subsequently, the microencapsulation of theranostic AuNPs in core-shell structured microspheres via coaxial electrospraying was investigated. During co-axal electrospraying, a stable jet was formed as the applied high volage could bring about electrostatic stretch to the compound liquid coming out of the coaxial nozzle and overcome its surface tension[40], finally resulting in the formation of uniform microspheres when the solvent evaporated (Fig. 2d). It was observed under TEM that the coaxial electrosprayed PLGA50/50 microspheres possessed an obvious core-shell structure, where the theranostic AuNPs could be found in the meso-cores of the microspheres (Fig. 2e). It should be noted that the original structures of AuNPs that showed nanoscale surface roughness were well preserved for the encapsulated AuNPs (Fig. 2f), indicating effective and successful microencapsulation of theranostic AuNPs via coaxial

electrospraying and the high potential for realizing theranostic functions of the encapsulated AuNPs.

### 2.2 Localized delivery of theranostic NPs from multifunctional nanofibrous scaffolds

On the basis of successful synthesis of theranostic AuNPs and also encapsulation of the theranostic AuNPs in biodegradable PLGA microspheres for their controlled delivery, multifunctional nanofibrous scaffolds were fabricated through concurrent electrospinning (for generating PLGA75/25 nanofibers) and coaxial electrospraying (for generating theranostic AuNP-encapsulated PLGA50/50 microspheres). These new composite scaffolds displayed hierarchical architectures (Fig. 3a), showing an ECM-mimicking nanofibrous matrix (which was similar to that of neat electrospun PLGA 75/25 scaffolds (Fig. S4)) proven to be favorable for promoting tissue repair/regeneration[10-12], and also randomly dispersed PLGA50/50 microspheres within the nanofibrous PLGA75/25 matrix which acted as delivery vehicles for theranostic AuNPs. These dispersed PLGA50/50 microspheres in scaffolds (Fig. 3b) had similar morphology and structure (the majority of them showing diameters of ~5 μm) to those of microspheres formed through the coaxial electrospraying operation alone (Fig. 2d). Since the average pore size (1082±294 nm) of the electrospun nanofibrous PLGA75/25 matrix was smaller than the average diameter (~5 μm) of the coaxial electrosprayed PLGA50/50 microspheres, the microspheres could be stably fixed within the nanofibrous matrix of the multifunctional scaffolds. Most of these microspheres would not become loose during scaffold manufacture and subsequent handling because they had been covered/secured by overlaying nanofibers. In addition, although PLGA microspheres had been embedded in the nanofibrous

structures, the multifunctional nanofibrous scaffolds formed via the concurrent electrospinning and coaxial electrospraying still presented comparable mechanical properties (Young's modulus: 12.1 ± 1.1 MPa, UTS: 1.52 ± 0.05 MPa, and fracture strain: 35.6 ± 6.2 %) as compared to the neat electrospun PLGA75/25 nanofibrous scaffolds (Young's modulus: 10.9 ± 0.3 MPa, UTS: 1.71 ± 0.08 MPa, and fracture strain: 43.2 ± 5.9 %) (Fig. 3c), indicating excellent structural integrity of the composite scaffolds made in the current study using the concurrent manufacturing process.

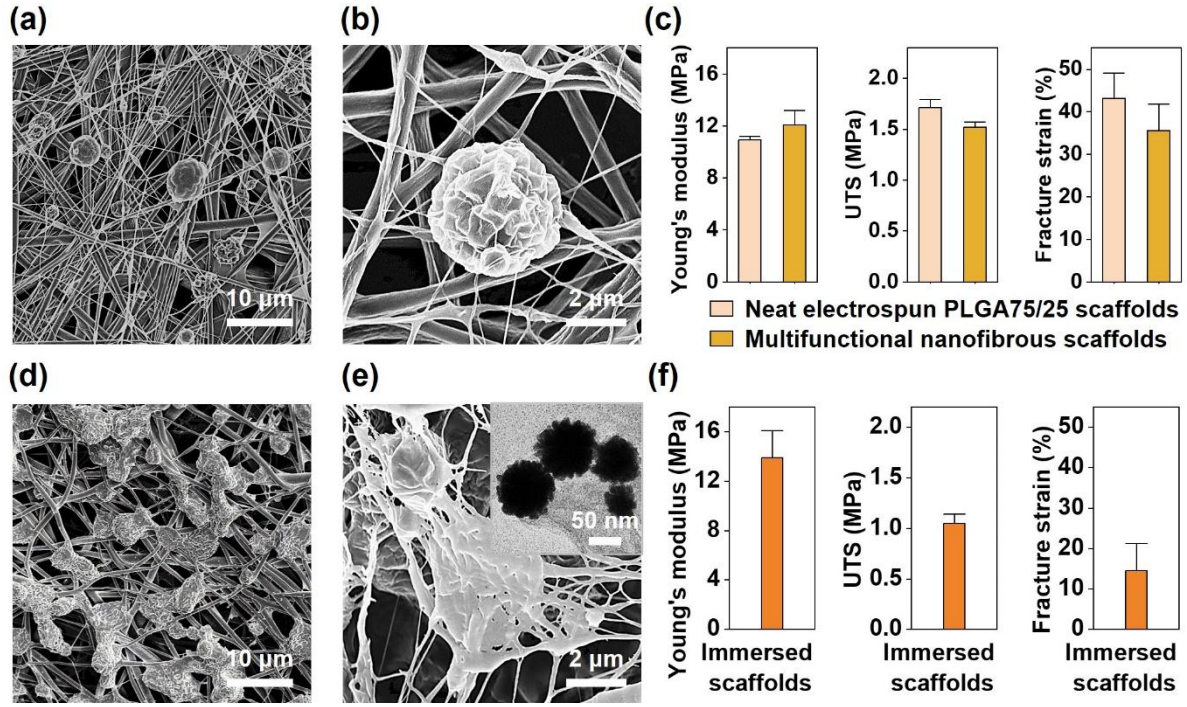


**Figure 3 Formation, structure, and properties of multifunctional nanofibrous scaffolds.** (a, b) Morphology and structure of multifunctional nanofibrous scaffolds observed under SEM at low (a) and high (b) magnifications. (c) Mechanical properties (Young's modulus, UTS, and fracture strain) of multifunctional scaffolds and neat electrospun PLGA75/25 scaffolds. (d) Morphology and structure of multifunctional

nanofibrous scaffolds after a 3-day immersion treatment. (e) Morphology and structure of multifunctional nanofibrous scaffolds after a 21-day immersion treatment, with the insert showing the structure of theranostic AuNPs collected in the immersion medium. (f) Mechanical properties (Young's modulus, UTS, and fracture strain) of multifunctional nanofibrous scaffolds after an immersion treatment.

As the localized delivery of theranostic AuNPs from break-up microspheres (owing to their biodegradation *in vitro* or *in vivo*) is essential for the fulfillment of diagnosis-and-therapy functions of the multifunctional nanofibrous scaffolds developed in the current study, experiments were conducted to investigate the morphological changes of scaffolds and the release of theranostic AuNPs in a physiologically mimicking environment, i.e., immersing samples in phosphate buffer saline (PBS) at 37 °C in a shaking water bath. Due to different biodegradation rates between PLGA50/50 and PLGA75/25[19], after a 3-day immersion treatment, the PLGA50/50 microspheres dispersed in the PLGA75 fibrous matrix of multifunctional scaffolds had shown obvious morphological and structural changes, resulting from the gradual swelling and degradation of PLGA50/50, while the nanofibrous structure of PLGA75/25 matrix of the scaffolds was still maintained (Fig. 3d). Some nano- and submicron-pores could be observed on the surface of microspheres after immersion (Fig. 3d), which could offer possible outlets for the release of encapsulated theranostic AuNPs from the microspheres. As for the scaffolds after a 21-day immersion treatment, the microspheres in the scaffolds completely broke up (Fig. 3e), which would allow the total release of encapsulated theranostic AuNPs. Even after the 21-day immersion treatment, having been collected from the immersion

medium, monodispersed theranostic AuNPs with negligibly changed structures were seen (insert of Fig. 3e), implying the potential long "circulation lifetime" for well-preserved theranostic AuNP as a consequence of controlled, sustained local delivery via the multifunctional nanofibrous scaffolds. The *in vitro* degradation behavior was compared between multifunctional nanofibrous scaffolds and neat electrospun PLGA75/25 scaffolds through immersion treatments (in PBS and at 37 °C). Owing to relatively faster hydrolysis of PLGA50/50 than PLGA75/25[35], it was observed that the *in vitro* degradation rate of multifunctional nanofibrous scaffolds was slightly higher than that of neat electrospun PLGA75/25 scaffolds (Fig. S5). Even with the relatively faster degradation of PLGA50/50 microspheres after the 21-day immersion treatment, the PLGA75/25 matrix of scaffolds still showed a nanofibrous architecture (Fig. 3e) and the scaffolds could still provide suitable mechanical properties (Young's modulus: 13.9 ± 2.2 MPa, UTS: 1.05 ± 0.09 MPa, and fracture strain: 14.5 ± 6.8 %) (Fig. 3f) for soft tissue engineering[41]; hence the scaffolds appeared to be able to provide stable structural and mechanical supports for the repair/regeneration of soft tissues.

### 2.3 Hemocompatibility and cytocompatibility

Because the multifunctional nanofibrous scaffolds would have direct contact with blood and biological cells upon their implantation in the surgically resected tissue sites for providing diagnosis-to-therapy functions, these scaffolds must have excellent biocompatibility, i.e., hemocompatibility and cytocompatibility, to ensure biosafety. To assess the hemocompatibility of multifunctional nanofibrous scaffolds, examinations were conducted

firstly on the aggregation behavior of blood cells, including red blood cells (RBCs), white blood cells (WBCs) and platelets, when reacting with aqueous extracts from the scaffolds. The aqueous extracts were obtained by immersing multifunctional nanofibrous scaffolds or theranostic NP-free scaffolds in PBS for 3 days (which was the time point when theranostic AuNPs started to be released from multifunctional nanofibrous scaffolds in PBS). When reacting with blood cells, aqueous extracts from neither scaffold types would cause abnormal aggregation of RBCs, WBCs, or platelets (Fig. 4a). These results suggested that the scaffolds, either composed of pristine polymers or with the incorporation of theranostic NPs, would not induce pathologically relevant aggregation of blood cells, such as blood coagulation as a consequence of activating platelet aggregation. Also, percentages of hemolysis were calculated for multifunctional nanofibrous scaffolds and theranostic NP-free scaffolds based on the aqueous extracts collected after the 3-day immersion treatment. It was found that the aqueous extracts of both scaffold types resulted in negligible hemolysis (<1%) when PBS and distilled water were used as the negative control and the positive control, respectively. There was neither significant statistical difference between the two types of scaffolds regarding hemolysis (Fig. 4b). The results for blood cell aggregation and hemolysis analysis indicated excellent hemocompatibility for multifunctional nanofibrous scaffolds.

For studying the cytocompatibility of scaffolds, a primary cell, human umbilical vein endothelial cell (HUVEC), was seeded on multifunctional nanofibrous scaffolds, theranostic NP-free scaffolds and tissue culture plates (TCPs) and cultured at 37 °C in a 5 v/v% $CO_2$ atmosphere incubator. The viability and density of HUVECs on different samples after 1-, 3-, and 7-day culture were examined using Live/Dead cell viability assays. After cell staining, it

was observed that HUVECs could attach well and grow on scaffolds (both multifunctional nanofibrous scaffolds and theranostic NP-free scaffolds), with negligible differences as compared to cells growing on TCPs (Fig. 4c). With culturing for 1, 3, and 7 days, HUVECs showed to have excellent viability (>97%) for the two types of scaffolds and TCP that were tested, while there was no significant statistical difference among the tested samples at each time point (Fig. 4d). Regarding the cell density of HUVECs on scaffolds and TCP with different culture time, it was observed that HUVECs could grow and proliferate well on all samples tested. Also, there was no significant statistical difference in cell density among different samples (i.e., scaffolds and TCP) after 1-, 3-, and 7-day of incubation (Fig. 4e). These results suggested that multifunctional nanofibrous scaffolds, even with the incorporation of theranostic NPs, possessed the desired cytocompatibility for supporting cell attachment, survival, and proliferation.

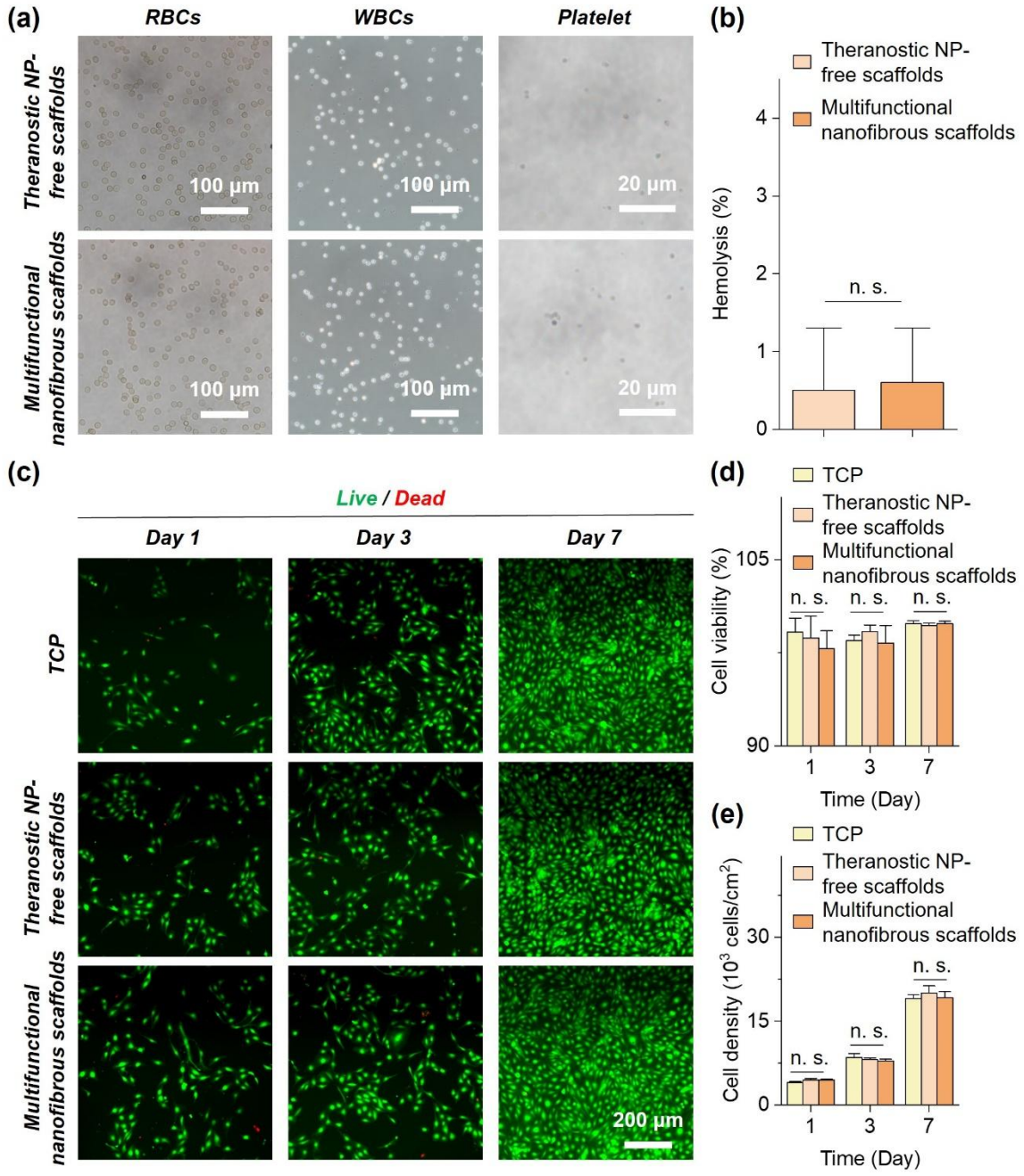


**Figure 4 Hemocompatibility and cytocompatibility of multifunctional nanofibrous scaffolds.** (a) Aggregation behaviors of RBCs, WBCs and platelets when reacting with aqueous extracts generated from multifunctional nanofibrous scaffolds and theranostic NP-free scaffolds. (b) Percentages of hemolysis caused by multifunctional nanofibrous scaffolds and theranostic NP-free scaffolds via the

aqueous extracts. (c) Representative fluorescence microscopic images of HUVECs cultured on multifunctional nanofibrous scaffolds, theranostic NP-free scaffolds, and TCPs, respectively, for 1, 3, and 7 days, which were stained with a Live/Dead cell viability assay kit. (Live cells were stained green; dead cells were stained red.) (d) Cell viability (percentages of live cells) for HUVECs cultured on the multifunctional nanofibrous scaffolds, theranostic NP-free scaffolds and TCPs for 1, 3, and 7 days. (e) Cell density for HUVECs cultured on multifunctional nanofibrous scaffolds, theranostic NP-free scaffolds and TCPs for 1, 3, and 7 days. (No significance (n. s.): $p > 0.05$, statistical analysis using one-way ANOVA with t-test.)

**2.4 Active targeting at targeted cancer cells**

To examine the targeting performance of theranostic AuNPs released from the multifunctional nanofibrous scaffolds, HeLa cells (with over-expressing folate receptors) or MCF-7 cells (without over-expressing folate receptors) were separately cultured with multifunctional scaffolds. Through 3-day co-incubation and then dark-field microscopic observation, it was found that MCF-7 cells, providing only non-specific binding with the released theranostic AuNPs, only displayed weak yellow signals (upper image in Fig. 5a), indicating a low level of cellular uptake of the theranostics. In contrast, clusters of strong yellow signals could be abundantly observed in the cytoplasm of HeLa cells cultured with multifunctional scaffolds for 3 days (lower image in Fig. 5a), indicating a high-efficiency cellular uptake of the theranostics released from multifunctional nanofibrous scaffolds which was due to the specific ligand-

receptor interactions[32]. Since the R6G embedded in the polymeric shell of theranostic AuNPs gave bright red fluorescence, a much higher level of uptake of theranostic AuNPs from the scaffolds by HeLa cells than by MCF-7 cells could also be observed under fluorescence microscopy, where much stronger red fluorescent signals were seen for HeLa cells cultured with multifunctional scaffolds for 3 days (Fig. 5b). With a longer culture time of 7 days, even stronger red fluorescent signals were observed for HeLa cells (Fig. S6), revealing sustained delivery of theranostic AuNPs from scaffolds and continuous accumulation of theranostic AuNPs in targeted cancer cells. The endocytosis and accumulation of theranostic AuNPs into the cytoplasm by HeLa cells were supported and confirmed by TEM observations. There were abundant theranostic AuNPs with well-preserved structures inside the cytoplasm of HeLa cells after 3-day co-incubation (Fig. 5c). A larger amount of theranostic AuNPs could be seen in the cytoplasm of HeLa cells after 7-day co-incubation (Fig. S7). The above results have shown not only sustained delivery of theranostic AuNPs by multifunctional nanofibrous scaffolds but also active targeting of the locally delivered theranostic AuNPs from the scaffolds at the targeted cancer cells with over-expressing folate receptors (the HeLa cells).

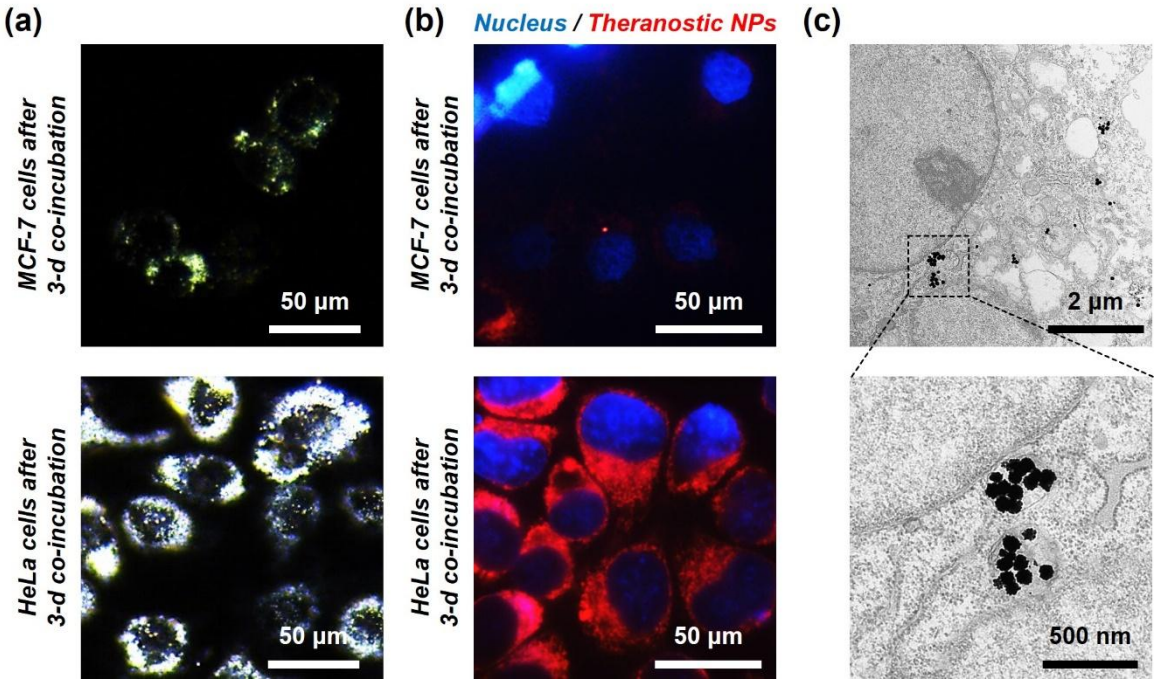


**Figure 5 Active targeting and cellular uptake of theranostic AuNPs released from multifunctional nanofibrous scaffolds by HeLa cells through *in vitro* experiments.** (a, b) Comparisons in dark-field (a) and fluorescence (b) microscopic images between non-specific binding to MCF-7 cells and active targeting at HeLa cells by theranostic AuNPs delivered by multifunctional nanofibrous scaffolds after 3-day co-incubation of cells and multifunctional scaffolds. (c) TEM images showing cellular uptake of theranostic AuNPs by HeLa cells after 3-day co-incubation of HeLa cells and multifunctional scaffolds.

### 2.5 SERS-based cancer detection and NIR-mediated photothermal cancer therapy

With the demonstration of strong active targeting capability of theranostic AuNPs locally delivered by multifunctional nanofibrous scaffolds, it was natural to proceed to examine the *in vitro* performance of the scaffolds for SERS-based cancer detection and NIR-mediated

photothermal cancer therapy. Since the cancer detection function of the scaffolds depended on the SERS activity of locally delivered theranostic AuNPs, the SERS signals of theranostic AuNPs released from the scaffolds were measured. It was found that there were no major differences in SERS signals (characteristic peaks at 613, 772, 1183, 1306 and 1500 $cm^{-1}$) between freshly synthesized theranostic AuNPs and those released from multifunctional scaffolds (Fig. 6a), demonstrating the well-preserved high SERS activity of theranostic AuNPs released from the scaffolds which formed the important base for cancer detection by the scaffolds. SERS measurement for the HeLa cells cultured with multifunctional nanofibrous scaffolds for 3 days was also conducted. Along with abundant uptake of theranostic AuNPs by HeLa cells after co-incubation, the labelled cells (viz., cells with internalized AuNPs) also exhibited sufficiently amplified Raman signals (Fig. 6a), suggesting promise of multifunctional nanofibrous scaffolds for early cancer diagnosis[42].

In additional to having high SERS activity, the theranostic AuNPs were also found to show strong and characteristic SPR absorption in the NIR region. When the wavelength of a light falls within the NIR band that can excite SPR of AuNPs, efficient energy conversion from light to heat will occur[43]. The theranostic AuNPs synthesized for the current study have been shown to be excellent therapeutic agent for NIR-mediated photothermal cancer therapy in the previous section as well as in our pervious study[31]. To evaluate the multifunctional nanofibrous scaffolds for the provision of photothermal cancer therapy, HeLa cells were cultured with the scaffolds for 3 days and subsequently the viability of Hela cells under an NIR irradiation (of the wavelength of 785 nm) after the removal of scaffolds was investigated. Upon the NIR irradiation using a laser beam of a relatively low power density (2.0 $mW/cm^2$), the viability of

the HeLa cells was not affected (Fig. S8), suggesting good biosafety of the multifunctional nanofibrous scaffolds and localized delivery of theranostic AuNPs. When the power density of the laser beam was increased to 5.3 mW/cm$^2$, it was found that HeLa cells cultured with multifunctional nanofibrous scaffolds for 3 days were nearly completely killed at the site exposed to the NIR irradiation (Fig. 6b). In contrast, the viability of HeLa cells at the NIR exposure site was not changed when the had been cultured with theranostic AuNP-free scaffolds (Fig. 6b). This difference in HeLa cell viability observed through the two sets of experiments suggested that (1) cell death was caused by the NIR-mediated photothermal effect of the theranostic AuNPs delivered locally from the scaffolds, rather than the NIR irradiation itself; and (2) with good cellular uptake of the theranostic AuNPs delivered locally from the scaffolds, sufficient NIR laser power and NIR-mediated PTT that was based on SPR absorption of AuNPs, HeLa cells could be killed upon NIR laser exposure. It should also be noted that, interestingly, for all HeLa cells cultured with multifunctional nanofibrous scaffolds, only cells within the area that was exposed to the NIR laser were killed, showing a high spatial resolution for the photothermal cancer therapy adopted in the current study. Combining the laser energy-dependent and high-resolution features of the PTT in cancer cell ablation, the multifunctional nanofibrous scaffolds developed in the current study hold high promise for providing precise cancer therapy with minimal side effects[44]. This article focuses on the cancer targeting, sensing and therapy part of the multifunctional scaffolds, while the tissue regeneration capability of the multifunctional scaffolds is reported separately in another article.

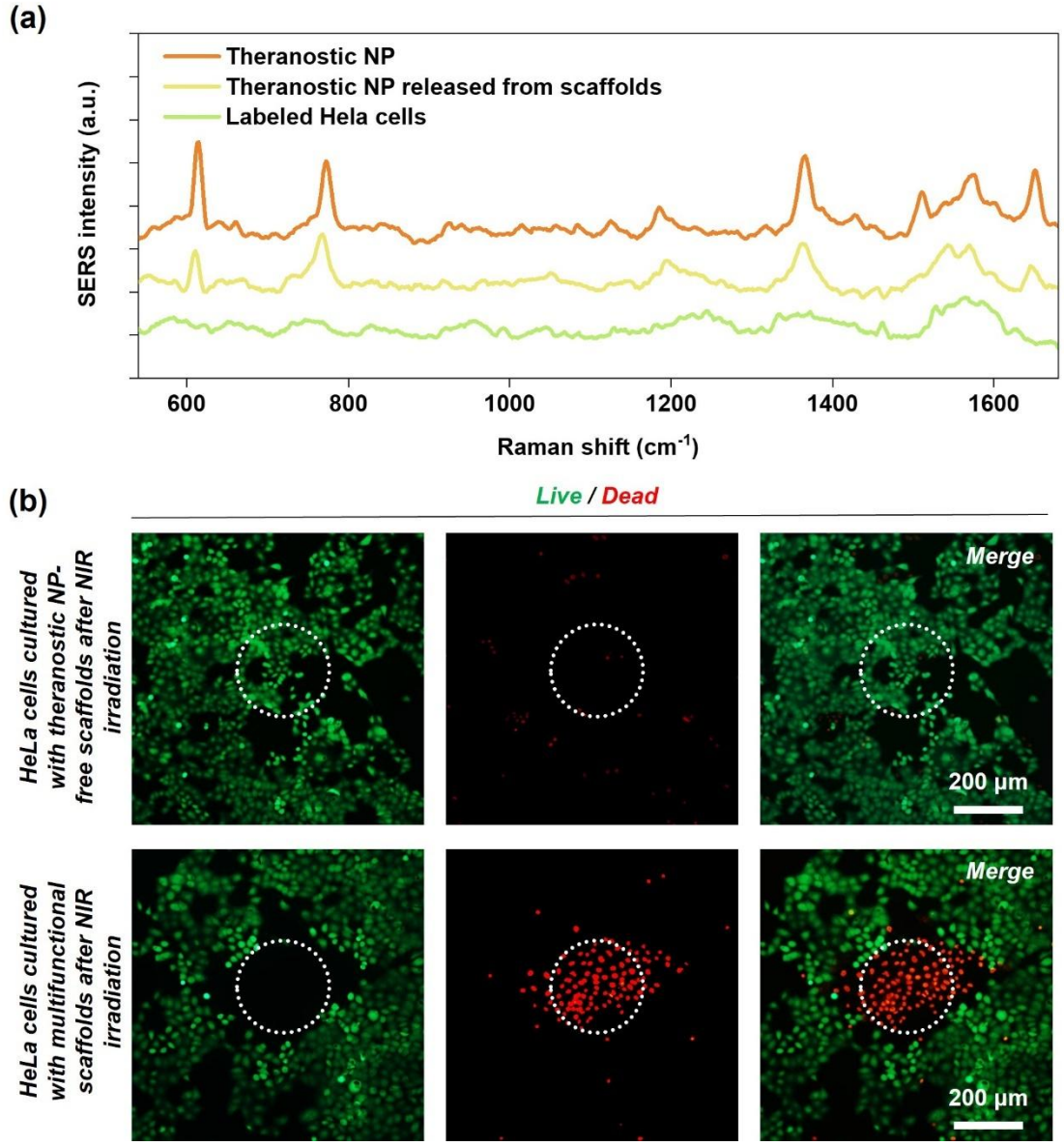


**Figure 6 SERS detection and NIR-mediated PTT for cancer cells achieved by multifunctional nanofibrous scaffolds.** (a) SERS spectra of as-fabricated theranostic AuNPs, theranostic AuNPs released from scaffolds, and HeLa cells after the uptake of theranostic AuNP through a 3-day co-incubation of cells and multifunctional scaffolds. (b) Representative fluorescence images of HeLa cells, as stained by Calcein AM and Ethd-1, upon NIR laser irradiation at the laser power density of 5.3 mW/cm$^2$, with the cells having been cultured with multifunctional

scaffolds or theranostic NP-free scaffolds for 3 days. Dashed circles indicate the sites irradiated by the laser beam.

## 3. Conclusions

In this study, multifunctional nanofibrous scaffolds capable of localized delivery of theranostic NPs have been produced through concurrent electrospinning and coaxial electrospraying. These scaffolds possess an ECM-mimicking nanofibrous architecture and soft tissue-like mechanical properties, which is suitable for the repair/regeneration of soft tissues of the body. They exhibit excellent hemocompatibility and cytocompatibility, ensuring biosafety after implantation in the human body. Importantly, these scaffolds also allow localized delivery of theranostic AuNPs with well-preserved structures and characteristics, creating the equivalent of a prolonged circulation time of at least 21 days for the theranostic AuNPs. Through the localized delivery of theranostic AuNPs, the multifunctional nanofibrous scaffolds have shown the desired and designed functions, including active targeting at targeted cancer cells, SERS-based cancer detection and NIR-mediated photothermal cancer therapy, holding the high promise for adaptive postoperative cancer managements. Also, the research performed in this study offers insights into nanoparticle microencapsulation via electrospraying, which may open new avenues for the applications of functional nanoparticles in healthcare, environmental, and safety fields[45].

## 4. Experimental Section

***Materials*** Dicyclohexylcarbodiimide (DCC), hydroxysuccinimide (NHS), a low molecular weight CS, FA, R6G, and chloroauric acid ($HAuCl_4 \cdot 3H_2O$) were purchased from Sigma-Aldrich, USA. The organic solvents, dimethyl sulfoxide (DMSO) and dichloromethane (DCM), were products of Fisher Scientific, USA. PLGA75/25 and PLGA50/50, both having the inherent viscosity of 0.6-0.8 dL/g, were supplied by Lakeshore Biomaterials, USA. Deionized (DI) water used in the experiments was obtained from a DI water producer (Model D12681, Barnstead International, USA). Cervical carcinoma cell line (HeLa cell) and breast cancer cell line (MCF-7 cell) were supplied by ATCC, USA.

***Synthesis of theranostic NPs*** The theranostic NPs, i.e., R6G-embedded and CS-FA-capped AuNPs, were synthesized by using the one-pot synthesis method previously established by our group[31]. Briefly, a mixture solution was made by mixing FA, DCC and NHS in DMSO under stirring at room temperature for 12 h in the dark, which was then slowly added into a CS solution (CS dissolved in 1.0 w/v% acetate buffer), followed by stirring at room temperature for 16 h in the dark to form FA-conjugated CS. The FA-conjugated CS solution (3.0 mg/mL, in 1.0 w/v% acetate buffer) was then mixed with a $HAuCl_4$ aqueous solution (1.0 mM) at a volume ratio of 5:1. The mixture solution was heated to 90 °C for 3 h under stirring. After the 3-h reaction, R6G was added into the mixture solution with a final concentration of 0.1 M. After an additional 12-h stirring at room temperature in the dark, particle collection through centrifuging, and rinsing with DI water for 3 times, theranostic AuNPs were obtained.

***Fabrication of theranostic NP-encapsulated microspheres*** A coaxial nozzle consisting of an inner capillary and an outer capillary was employed in coaxial electrospraying for making core-shell structured microspheres. PLGA50/50 was dissolved in DCM to form a polymer solution with a PLGA50/50 concentration of 5.0 w/v%, which would be connected to the outer capillary of the coaxial nozzle. A theranostic AuNP-suspended aqueous solution (0.5 mM) would be fed by the inner capillary. On the basis of our previous work[35], optimized processing parameters (applied voltage: 15.0 kV, working distance: 15.0 cm, feeding rate for the outer PLGA50/50 solution: 2.03 mL/h, feeding rate for the inner theranostic AuNP-suspended aqueous solution: 0.76 mL/h) were used for coaxial electrospraying, resulting finally in solidified microspheres after solvent evaporation. Diameters of the microspheres were measured and analyzed using the ImageJ software.

***Fabrication of multifunctional nanofibrous scaffolds*** The multifunctional nanofibrous scaffolds, comprising electrospun PLGA75/25 fibers and coaxial electrosprayed theranostic AuNP-encapsulated PLGA50/50 microspheres, were fabricated through the established concurrent electrospinning and coaxial electrospraying process[36]. In brief, a 15.0 w/v% PLGA75/25 solution was firstly prepared by dissolving the polymer in DCM. Electrospinning of the PLGA75/25 solution at a high voltage of 15.0 kV, a working distance of 10.0 cm and a feeding rate of 2.0 mL/h was conducted concurrently with coaxial electrospraying described above. After co-deposition of electrospun PLGA75/25 fibers and coaxial electrosprayed theranostic AuNP-encapsulated PLGA50/50 microspheres on a grounded rotating drum collector, the multifunctional nanofibrous scaffolds were obtained.

***Morphological, structural, spectral, and mechanical characterization*** The morphologies and structures of theranostic AuNPs, coaxial electrosprayed microspheres, and multifunctional nanofibrous scaffolds were characterized by using a scanning electron microscope (LEO 1530 field emission SEM, Gemini, Germany), a transmission electron microscope (Tecnai G2 20S-TWIN TEM, FEI, USA), a dark-field microscope (Leica DMi8, Germany) and a fluorescence microscope (Fluoview FV 1000, Olympus, Japan). The samples for SEM observations were firstly coated by a thin layer of gold via sputtering. The morphologies and structures of multifunctional nanofibrous scaffolds and neat electrospun PLGA 75:25 scaffolds were studies using SEM, with fiber diameters and scaffold pore sizes (which corresponded to characteristic distances between fibers) being measured and analyzed using the ImageJ software. The samples for TEM observations were collected directly on copper grids covered with a thin carbon film. The size distribution of theranostic AuNPs were studied using a Particle Analyzer (Bruker Tensor 2, Bruker Optics, Germany). The spectral absorption of theranostic AuNPs in the region from ultraviolet (UV) to NIR (wavelength: 365-900 nm) was analyzed by using a UV-visible spectrophotometer (Lambda 20, Perkin Elmer, USA). The Raman signals of theranostic AuNPs were measured by using a Raman microscope (HORIBA LabRAM HR Evolution, France), while signals of pure R6G was also measured as the control. To evaluate the mechanical properties of different types of scaffolds, including the neat electrospun PLGA75/25 nanofibrous scaffolds, as-fabricated multifunctional nanofibrous scaffolds and multifunctional nanofibrous scaffolds during the 21-day immersion treatment (which was used for *in vitro* scaffold degradation, particularly for microspheres degradation, see below), tensile tests were performed on a tabletop Instron Micro Tester (Model 5848, USA) according to the

ASTM test standard (ASTM C1557). Tensile stress-strain curves were obtained, from which the Young's modulus, ultimate tensile strength (UTS) and fracture strain of different scaffolds were calculated.

***In vitro degradation assessment*** *In vitro* degradation of multifunctional scaffolds was studied by immersing pre-weighed samples in the immersion medium (PBS, supplemented with 0.02 w/v% sodium azide) in sealed bottles that were placed in a 37 °C shaking water bath. The immersion medium was refreshed every 2 days. The morphological changes of these immersed samples over different immersion times were examined under SEM after collecting the immersed samples, rinsing them with DI water for 3 times, and then freeze-drying for 48 h. Also, samples collected over different immersion times were dried and weighed. Curves showing weight loss percentages of scaffold samples with respect to immersion time were then plotted. Mechanical tests of *in vitro* degraded samples were conducted, as described above.

***Cell culture*** HeLa cells and MCF-7 cells, having respectively a high-level and a low-level expression of folate receptor, were cultured in the experiments. Both types of cells were expanded using dulbecco's modified eagle medium (DMEM) supplemented with 10.0 v/v% fetal bovine serum (FBS) and 100 units/mL penicillin-streptomycin (P/S) at T-75 cell culture flasks, maintained in a 37 °C incubator pumped with 5.0 v/v% $CO_2$ atmosphere. At 60-80% cell confluence, the cells were trypsinized and then seeded onto the scaffolds (theranostic NP-incorporated scaffolds or theranostic NP-free scaffolds) at the cell density of $3.0\times10^4$ cells/well in a 24-well tissue culture plate. The scaffolds were sterilized by a $^{60}$Co γ-irradiation with an intensity of 15.0 kGy for 30 mins prior to cell culture experiments.

***Hemocompatibility assays*** To evaluate the hemocompatibility of multifunctional nanofibrous scaffolds, blood cell aggregation and hemolysis tests were conducted according to established studies[46], with minor modifications. To investigate the blood cell aggregation, RBCs, WBCs and platelets were isolated from a healthy human's anticoagulated blood sample provided by a male volunteer with informed consent. They were then cultured in the immersion solutions obtained upon immersing sterilized samples (multifunctional nanofibrous scaffolds and theranostic NP-free scaffolds) in PBS for 3 days. In brief, RBCs were separated by centrifuging the anticoagulated whole blood at 700 rpm for 10 mins. Collected pellet was washed twice with Hank's balanced salt solution (HBSS, no calcium, no magnesium, no phenol red, Gibco, UK) and then suspended with HBSS with supplemented fetal bovine serum (FBS, 10 v/v%) at the volume ratio of 1:4. WBCs were isolated from the anticoagulated whole blood by pipetting the WBC-rich layer from the blood after the centrifugation. The isolated WBC-rich suspension was then centrifuged at 2,000 rpm for 10 mins, washed twice with HBSS, and then suspended with the FBS-supplemented HBSS. To isolate platelets, the anticoagulated whole blood was firstly centrifuged at 1,500 rpm for 12 min. The upper platelet-rich plasma was pipetted, centrifuged at 3,500 rpm for 5 min, and washed twice with HBSS. The pellet was then suspended by using the BS-supplemented HBSS. The collected cell suspensions (RBCs, WBCs, or platelets) were mixed with the immersion solutions at the volume ratio of 1:1. Upon incubation at 37 °C in a 5 v/v% $CO_2$ atmosphere incubator for 20 min, the RBCs, WBCs, and platelets treated with the immersion solutions obtained from different scaffolds in a 24-well cell culture plate were examined using an inverted optical microscope (Ti-U, Nikon, Japan).

Hemolysis assays were also performed for multifunctional nanofibrous scaffolds and theranostic NP-free scaffolds. In brief, immersion solutions, which were generated by immersing multifunctional nanofibrous scaffolds or theranostic NP-free scaffolds in PBS overnight, were firstly collected. 100 μL of each immersion solution, a negative control (PBS), and a positive control (distilled water) were separately mixed with a diluted blood sample (by diluting 100 μL of anticoagulated blood with 800 μL of PBS), which were then incubated at 37 °C in a 5 v/v% $CO_2$ atmosphere incubator for 30 min. Afterwards, the incubated samples were centrifuged at 700 rpm for 5 mins. The supernatant of each sample was collected, whose absorbance ("Absorb") at 541 nm was measured using a microplate reader (Molecular Devices Cmax Plus, USA). The hemolysis ratio was calculated according to the following equation:

$$\text{Hemolysis ratio (\%)} = (\text{Absorb}_{\text{sample}} - \text{Absorb}_{\text{negative}}) / (\text{Absorb}_{\text{positive}} - \text{Absorb}_{\text{negative}}) \times 100\% \quad (1)$$

where $\text{Absorb}_{\text{sample}}$, $\text{Absorb}_{\text{negative}}$, and $\text{Absorb}_{\text{positive}}$ were the absorbance at 541 nm of samples (N=3), negative control, and positive control, respectively.

***Cytocompatibility assessment*** To assess the cytocompatibility of multifunctional nanofibrous scaffolds, HUVECs (passage 2~3, ScienCell Research Laboratories, USA) were seeded on UV-sterilized scaffolds (1 cm × 1 cm) at a cell density of $5\times10^3$ cells/piece and then cultured at 37 °C in a 5 v/v% $CO_2$ atmosphere incubator. Theranostic NP-free scaffolds and blank tissue culture plates (TCPs) were used as controls. After 1, 3, and 7 days of incubation, HUVECs cultured with each scaffold sample and control were stained by using a Live/Dead viability kit (Molecular Probes, USA), where live and dead cells would be stained by calcein acetoxymethylester (Calcein AM) and ethidium homodimer-1 (Ethd-1), respectively, in the kit.

The cell-stained samples and controls were observed using the inverted microscope. The cell viability (percentage of live cells, %), as well as cell density (cells/mm$^2$), for each sample was calculated using the pictures (N =3) captured by the inverted microscope and the software Image J.

***Examination of cancer cell targeting*** After 3 days of incubation with multifunctional nanofibrous scaffolds, HeLa cells and MCF-7 cells were washed, fixed with a 4 v/v% paraformaldehyde (PFA) solution, and then observed under the dark-field microscope. Furthermore, HeLa cells and MCF-7 cells after culturing with multifunctional nanofibrous scaffolds for 3 days and 7 days were also observed under the fluorescence microscope, where the nuclei of cells were labeled by 4',6-diamidino-2-phenylindole (DAPI, Thermo Fisher Scientific, USA) and theranostic NP were revealed by the inherent fluorescence of embedded R6G.

***Evaluation of cellular uptake of theranostic NPs*** After 3 and 7 days of incubation with multifunctional nanofibrous scaffolds, HeLa cells were washed with ice-cold PBS for 3 times, trypsinized to be released and collected via centrifugation. The resultant cell blocks were fixed with a 4 v/v% PFA solution at 4 °C for 4 h, dehydrated using a series of aqueous ethanol solutions of gradient ethanol concentrations (50, 70, 90, and 100 v/v%) and then propylene oxide, and subsequently embedded in an epoxy resin. The embedded cell samples were sliced, which were then observed under TEM for investigating cellular uptake of theranostic AuNPs.

***In vitro SERS measurements*** To prepare specimens for *in vitro* SERS measurements, sterilized silicon wafers with the size of 5.0 mm × 5.0 mm were placed in the wells of a 24-well tissue

culture plate, subsequently seeded with HeLa cells at a cell seeding density of $3.0\times10^4$ cells/well, followed by putting a piece of sterilized theranostics-incorporated scaffolds in each well. After 3-day cell culture, the silicon wafers were taken out, washed 3 times with PBS, and then put under the Raman microscope for SERS measurements.

***In vitro photothermal experiments*** HeLa cells were cultured with the sterilized theranostic AuNP-incorporated scaffolds in a 24-well tissue culture plate with a cell density of $3.0\times10^4$ cells/well. After 3-day cell culture, the scaffolds were taken out from the wells. The cells were then irradiated by a NIR laser beam (wavelength of 785 nm) at the power density of 2.0 W/cm$^2$ or 5.3 W/cm$^2$ for 5 mins. The diameter of the laser spot was 320 μm. After NIR irradiation, cell viability assay was performed using the Live/Dead viability kit. The stained cells were observed under the fluorescence microscope. HeLa cells incubated with theranostic AuNP-free scaffolds and irradiated under the same conditions were used as control.

## Author Contribution Statement

Lin Guo: experimental investigation, writing; Qilong Zhao: experimental investigation, writing, editing; Li-wu Zheng: writing, reviewing; Min Wang: scaffold design, research supervision, writing, editing, reviewing.

## Conflict of Interest Statement

There are no conflicts of interest to declare.

## Supplementary Information

Supporting data are available online.


## Acknowledgements

M. Wang acknowledges the financial support for this work by Hong Kong's Research Grants Council (RGC) through research grants (17201017, 17200519 and N_HKU749/22) and by The University of Hong Kong (HKU) through grants in the Seed Fund for Basic Research Scheme. He also thanks a donor in Hong Kong for her generous donation to support his research in biomaterials and tissue engineering at HKU. L. Guo thanks HKU for providing her with a PhD scholarship. Assistance provided by members of M. Wang's research group at HKU and by technical staff in HKU's Department of Mechanical Engineering, Faculty of Dentistry and Electron Microscopy Unit is acknowledged.

Received: ((will be filled in by the editorial staff))

Revised: ((will be filled in by the editorial staff))

Published online: ((will be filled in by the editorial staff))

## References


1. L. A. Torre, F. Bray, R. L. Siegel, J. Ferlay, J. Lortet-Tieulent and A. Jemal, *CA Cancer J. Clin.*, 2015, **65**, 87-108.
2. A. Grzybowski, *New Engl. J. Med.*, 2012, **367**, 479-479.
3. N. Jiang, J. Y. Deng, X. W. Ding, B. Ke, N. Liu, R. P. Zhang and H. Liang, *World J. Gastroentero.*, 2014, **20**, 10537-10544.
4. O. Pech, A. Behrens, A. May, L. Nachbar, L. Gossner, T. Rabenstein, H. Manner, E. Guenter, J. Huijsmans and M. Vieth, *Gut*, 2008, **57**, 1200-1206.
5. C. E. DeSantis, C. C. Lin, A. B. Mariotto, R. L. Siegel, K. D. Stein, J. L. Kramer, R. Alteri, A. S. Robbins and A. Jemal, *CA Cancer J. Clin.*, 2014, **64**, 252-271.
6. R. Sauer, H. Becker, W. Hohenberger, C. Rodel, C. Wittekind, R. Fietkau, P. Martus, J. Tschmelitsch, E. Hager, C. F. Hess, J. H. Karstens, T. Liersch, H. Schmidberger, R. Raab and G. R. C. S. Grp, *New Engl. J. Med.*, 2004, **351**, 1731-1740.
7. J. S. Cooper, T. F. Pajak, A. A. Forastiere, J. Jacobs, B. H. Campbell, S. B. Saxman, J. A. Kish, H. E. Kim, A. J. Cmelak, M. Rotman, M. Machtay, J. F. Ensley, K. S. C. Chao, C. J. Schultz, N. Lee, K. K. Fu and R. T. O. G. 9501, *New Engl. J. Med.*, 2004, **350**, 1937-1944.
8. D. Porock, S. Nikoletti and F. Cameron, *Cancer Nurs.*, 2004, **27**, 71-78.
9. Y. Zhang and C. Jiang, *J. Control. Release*, 2021, **330**, 554-564.
10. C. Wang and M. Wang, *J. Mater. Chem. B*, 2017, **5**, 1388-1399.
11. Q. Zhao, J. Wang, H. Cui, H. Chen, Y. Wang and X. Du, *Adv. Funct. Mater.*, 2018, **28**, 1801027.
12. Q. Zhao, H. Cui, J. Wang, H. Chen, Y. Wang, L. Zhang, X. Du and M. Wang, *ACS Appl. Mater. Inter.*, 2018, **10**, 23583-23594.
13. J. W. Zhao and W. G. Cui, *Adv. Fiber Mater.*, 2020, **2**, 229-245.
14. K. M. Moore, A. B. Murthy, E. G. Graham-Gurysh, S. D. Hingtgen, E. M. Bachelder and K. M. Ainslie, *ACS Biomater. Sci. Eng.*, 2020, **6**, 3762-3777.
15. Z. Huang, Z. Tian, M. Zhu, C. Wu and Y. Zhu, *Adv. Therap.*, 2020, **4**, 2000212.
16. J. Li, J. Li, Y. Yao, T. Yong, N. Bie, Z. Wei, X. Li, S. Li, J. Qin, H. Jia, Q. Du, X. Yang and L. Gan, *Theranostics*, 2022, **12**, 3503-3517.
17. Y. W. Xi, J. Ge, M. Wang, M. Chen, W. Niu, W. Cheng, Y. M. Xue, C. Lin and B. Lei, *ACS Nano*, 2020, **14**, 2904-2916.
18. C. C. Xue, M. H. Li, L. Sutrisno, B. B. Yan, Y. Zhao, Y. Hu, K. Y. Cai, Y. L. Zhao, S. H. Yu and Z. Luo, *Adv. Funct. Mater.*, 2021, **31**, 2008732.
19. Y. Zhou, Q. Zhao, N. L. Y. Tsai and M. Wang, *MRS Commun.*, 2019, **9**, 413-420.
20. D. C. Niu, Y. S. Li and J. L. Shi, *Chem. Soc. Rev.*, 2017, **46**, 569-585.
21. D. Ho, X. L. Sun and S. H. Sun, *Acc. Chem. Res.*, 2011, **44**, 875-882.
22. Y. J. Liu, P. Bhattarai, Z. F. Dai and X. Y. Chen, *Chem. Soc. Rev.*, 2019, **48**, 2053-2108.
23. C. J. Murphy, A. M. Gole, J. W. Stone, P. N. Sisco, A. M. Alkilany, E. C. Goldsmith and S. C. Baxter, *Acc. Chem. Res.*, 2008, **41**, 1721-1730.
24. S. Sindhwani, A. M. Syed, J. Ngai, B. R. Kingston, L. Maiorino, J. Rothschild, P. MacMillan, Y. W. Zhang, N. U. Rajesh, T. Hoang, J. L. Y. Wu, S. Wilhelm, A. Zilman,

S. Gadde, A. Sulaiman, B. Ouyang, Z. Lin, L. S. Wang, M. Egeblad and W. C. W. Chan, *Nat. Mater.*, 2020, **19**, 566-575.
25. D. Peer, J. M. Karp, S. Hong, O. C. FaroKHzad, R. Margalit and R. Langer, *Nat. Nanotechnol.*, 2007, **2**, 751-760.
26. J. Langer, D. J. de Aberasturi, J. Aizpurua, R. A. Alvarez-Puebla, B. Auguie, J. J. Baumberg, G. C. Bazan, S. E. J. Bell, A. Boisen, A. G. Brolo, J. Choo, D. Cialla-May, V. Deckert, L. Fabris, K. Faulds, F. J. G. de Abajo, R. Goodacre, D. Graham, A. J. Haes, C. L. Haynes, C. Huck, T. Itoh, M. Ka, J. Kneipp, N. A. Kotov, H. Kuang, E. C. Le Ru, H. K. Lee, J. F. Li, X. Y. Ling, S. A. Maier, T. Mayerhofer, M. Moskovits, K. Murakoshi, J. M. Nam, S. Nie, Y. Ozaki, I. Pastoriza-Santos, J. Perez-Juste, J. Popp, A. Pucci, S. Reich, B. Ren, G. C. Schatz, T. Shegai, S. Schlucker, L. L. Tay, K. G. Thomas, Z. Q. Tian, R. P. Van Duyne, T. Vo-Dinh, Y. Wang, K. A. Willets, C. Xu, H. Xu, Y. Xu, Y. S. Yamamoto, B. Zhao and L. M. Liz-Marzan, *ACS Nano*, 2020, **14**, 28-117.
27. J. F. Li, Y. F. Huang, Y. Ding, Z. L. Yang, S. B. Li, X. S. Zhou, F. R. Fan, W. Zhang, Z. Y. Zhou, D. Y. Wu, B. Ren, Z. L. Wang and Z. Q. Tian, *Nature*, 2010, **464**, 392-395.
28. A. M. Alkilany, L. B. Thompson, S. P. Boulos, P. N. Sisco and C. J. Murphy, *Adv. Drug Deliv. Rev.*, 2012, **64**, 190-199.
29. X. H. Huang, I. H. El-Sayed, W. Qian and M. A. El-Sayed, *J. Am. Chem. Soc.*, 2006, **128**, 2115-2120.
30. J. C. Qiu, M. H. Xie, T. Wu, D. Qin and Y. N. Xia, *Chem. Sci.*, 2020, **11**, 12955-12973.
31. S. Y. Li and M. Wang, *IET Nanobiotechnol.*, 2012, **6**, 136-143.
32. Y. Teow and S. Valiyaveettil, *Nanoscale*, 2010, **2**, 2607-2613.
33. M. P. Nikitin, I. V. Zelepukin, V. O. Shipunova, I. L. Sokolov, S. M. Deyev and P. I. Nikitin, *Nat. Biomed. Eng.*, 2020, **4**, 717-731.
34. C. L. Zhang and S. H. Yu, *Chem. Soc. Rev.*, 2014, **43**, 4423-4448.
35. Q. Zhao and M. Wang, *Polym. Degrad. Stabil.*, 2019, **162**, 169-179.
36. Q. Zhao, Y. Zhou and M. Wang, *Acta Biomater.*, 2021, **123**, 312-324.
37. S.-Y. Li and M. Wang, *Mater. Lett.*, 2013, **92**, 350-353.
38. S. J. Ding, L. Ma, J. R. Feng, Y. L. Chen, D. J. Yang and Q. Q. Wang, *Nano Res.*, 2022, **15**, 2715-2721.
39. V. Shanmugam, S. Selvakumar and C. S. Yeh, *Chem. Soc. Rev.*, 2014, **43**, 6254-6287.
40. D. Wang, X. Zhao, Y. Lin, J. Liang, T. Ren, Z. Liu and J. Li, *Nanoscale*, 2018, **10**, 9867-9879.
41. C. F. Guimarães, L. Gasperini, A. P. Marques and R. L. Reis, *Nat. Rev. Mater.*, 2020, **5**, 351-370.
42. S. Siddhanta, C. Zheng, C. Narayana and I. Barman, *Chem. Sci.*, 2016, **7**, 3730-3736.
43. M. L. Brongersma, N. J. Halas and P. Nordlander, *Nat. Nanotechnol.*, 2015, **10**, 25-34.
44. M. R. K. Ali, Y. Wu and M. A. El-Sayed, *J. Phys. Chem. C*, 2019, **123**, 15375-15393.
45. M. Auffan, J. Rose, J. Y. Bottero, G. V. Lowry, J. P. Jolivet and M. R. Wiesner, *Nat. Nanotechnol.*, 2009, **4**, 634-641.
46. R. Augustine, P. Dan, A. Sosnik, N. Kalarikkal, N. Tran, B. Vincent, S. Thomas, P. Menu and Didier Rouxel. *Nano Res.*, 2017, **10**, 3358-3376.

Multifunctional scaffolds with an extracellular matrix (ECM)-like nanofibrous architecture, soft tissue-like mechanical properties, and capability of localized delivery of theranostic nanoparticles are highly promising tissue engineering patches for the repair and regeneration of tissues at the cancerous sites after surgery, while providing active targeting, diagnosis and photothermal therapy for potentially residual cancer cells, exhibiting high promise for adaptive postoperative cancer management.

*Lin Guo[1,†], Qilong Zhao[1,2,†], Li-wu Zheng[3], Min Wang[1,*]*

**Multifunctional Nanofibrous Scaffolds Capable of Localized Delivery of Theranostic Nanoparticles for Postoperative Cancer Management**

ToC figure: